Letter

Up and down quark structure of the proton

V. M. Abazov *et al.*[*]
(D0 Collaboration)

(Received 14 March 2024; revised 26 May 2024; accepted 29 September 2024; published 7 November 2024)

We report an improved measurement of the valence u and d quark distributions from the forward-backward asymmetry in the Drell-Yan process using 8.6 fb^{-1} of data collected with the D0 detector in $p\bar{p}$ collisions at $\sqrt{s} = 1.96$. This analysis provides the values of new structure parameters that are directly related to the valence up and down quark distributions in the proton. In other experimental results measuring the quark content of the proton, d quark contributions are mixed with those from other quark flavors. In this measurement, the u and d quark contributions are separately extracted by applying a factorization of the QCD and electroweak portions of the forward-backward asymmetry.

DOI: 10.1103/PhysRevD.110.L091101

In the constituent quark model, the valence u and d quarks comprise the proton. The valence u quark density has been determined from deep inelastic scattering (DIS) data, where the u quark contribution dominates in photon-exchange interactions [1–7]. However, the valence d quark density has not been well measured as most measurements are not predominantly sensitive to its contribution. Consequently, our knowledge of the valence d quark mainly comes from the global analysis of the parton distribution functions (PDFs), which depend strongly on the calculations of the perturbative quantum chromodynamics (QCD), the choice of formalism for the nonperturbative effects, and the sum rules [8–10].

It is difficult to have a d-quark-dominant measurement because the u and d quark contributions are always mixed and experimentally indistinguishable in neutral current interactions. In principle, measurements of the charge current DIS data could distinguish the u and d quarks in the initial state. However, these determinations have been either complicated by nuclear binding effects in the neutrino-iron interactions [11,12] or limited by the data sample size in lepton-proton interactions [13]. Recently, it was shown that the u and d quark information can be separated from electroweak effects and factorized into structure parameters, P_u and P_d, in the Drell-Yan process [14,15]. This factorization, valid to all orders of QCD, and the use of $p\bar{p}$ collisions allow for determination of valence quark distributions for specific quark flavors.

In this paper, we report a determination of P_u and P_d in $p\bar{p} \to Z/\gamma^* \to \ell^+\ell^-$ events using data corresponding to 8.6 fb^{-1} of integrated luminosity collected with the D0 detector at the Fermilab Tevatron at $\sqrt{s} = 1.96$ TeV. Our analysis provides a model-independent measurement of the u and d quark densities in the kinematic region where valence quarks are dominant.

The u and d quark contributions can be individually factorized in the forward-backward asymmetry, A_{FB}, of the $p\bar{p} \to Z/\gamma^* \to \ell^+\ell^-$ events, defined as

$$A_{FB} = \frac{N_F - N_B}{N_F + N_B}, \tag{1}$$

where N_F and N_B are the number of forward and backward events, defined as those for which $\cos\theta > 0$ and $\cos\theta < 0$, with θ defined as the angle between the direction of the negatively charged lepton and the direction of the proton beam in the Collins-Soper frame [16]. At specific values of the dilepton rapidity (Y) and transverse momentum (Q_T) defined with respect to the beam axis, the observed A_{FB} distribution as a function of the dilepton invariant mass (M) can be factorized as [14]

$$\begin{aligned} A_{FB}(M) &= \frac{\sum_{q=u,c}[1-2D_q(M)]\sigma_q(M)}{\sigma_{\text{total}}(M)} \cdot A^u_{FB}(M) \\ &\quad + \frac{\sum_{q=d,s,b}[1-2D_q(M)]\sigma_q(M)}{\sigma_{\text{total}}(M)} \cdot A^d_{FB}(M) \\ &\equiv \mathcal{C}_u(M)A^u_{FB}(M) + \mathcal{C}_d(M)A^d_{FB}(M), \end{aligned} \tag{2}$$

where σ_q is the subprocess cross section for a specific $q\bar{q}$ ($q = u, d, s, c, b$) initial state, σ_{total} is the total cross section $\sum_{q=u,d,s,c,b}\sigma_q$, and A^u_{FB} and A^d_{FB} are asymmetries for initial up-type states ($u\bar{u}$ and $c\bar{c}$) and down-type states

[*]Full author list given at the end of the article.

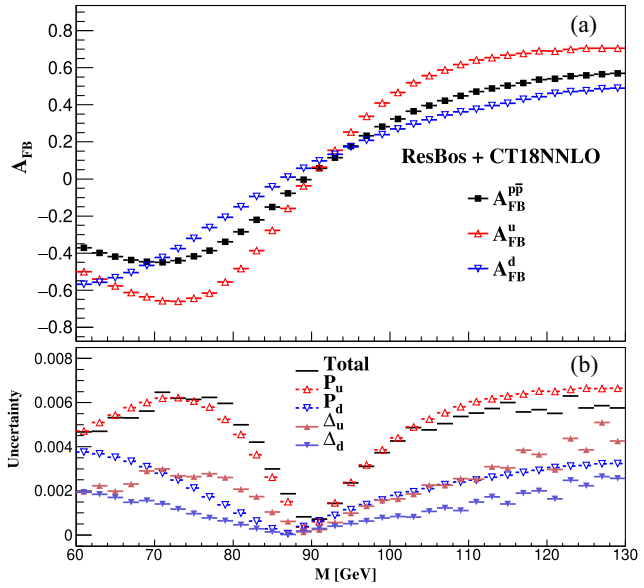

FIG. 1. (a) The PDF-independent A_{FB}^{u} and A_{FB}^{d} predicted by ResBos as a function of M and the resulting A_{FB} in $p\bar{p}$ collisions using the CT18NNLO PDF. (b) The PDF induced absolute uncertainties in A_{FB} due to P_u, P_d, Δ_u, and Δ_d.

($d\bar{d}$, $s\bar{s}$, and $b\bar{b}$), respectively. Forward and backward events for A_{FB}^{u} and A_{FB}^{d} are defined in the Collins-Soper frame in terms of a new angle θ' between the negatively charged lepton direction and the quark direction. The dilution factor D_q is defined as the probability for the $q\bar{q}$ subprocess to have an initial state where q comes from the antiproton while $\bar{q}$ comes from the proton, for which $\cos\theta = -\cos\theta'$.

Equation (2) factorizes the QCD part of the observed A_{FB} into $\mathcal{C}_u$ and $\mathcal{C}_d$, and the electroweak part as A_{FB}^{u} and A_{FB}^{d}, so that the observed A_{FB} is a combination of the two hard-process-level asymmetries with the proton structure information as their weights. Both A_{FB}^{u} and A_{FB}^{d} are determined by the effective weak mixing angle $\sin^2\theta_{\rm eff}^{\ell}$ and are independent of parton densities, but have different dependences on M due to the different Z-to-up and Z-to-down quark couplings. A_{FB}^{u} and A_{FB}^{d} can be precisely predicted. Figure 1(a) shows A_{FB}^{u} and A_{FB}^{d} as a function of M, calculated using ResBos [17] with CT18N NLO PDFs [8].

$\mathcal{C}_u$ and $\mathcal{C}_d$ can be averaged over a finite mass range to further separate them into mass-averaged structure parameters (P_u and P_d) and mass-dependent structure parameters (Δ_u and Δ_d) [14]:

$$\mathcal{C}_{u,d}(M) = P_{u,d} + \Delta_{u,d}(M). \tag{3}$$

In this analysis, P_u and P_d are defined by averaging over the dilepton mass range [70, 116] GeV. The Δ_u and Δ_d terms can be predicted with small uncertainties for M in this narrow window around the Z boson pole [14,15]. The uncertainties on A_{FB} due to the P_q and Δ_q parameters are shown in Fig. 1(b), indicating that P_q dominates the proton structure information in A_{FB}.

In this paper, we focus on the measurement of P_u and P_d, which can be determined by comparing Eqs. (2) and (3) to the measured A_{FB} distribution. The values of Δ_u and Δ_d are fixed to the CT18NNLO predictions. P_u and P_d contain both the dilution and the cross section parts. The dilution factors D_u and D_d are small since the interactions of an antiquark in the proton and a quark in the antiproton are suppressed in the relevant x range at the Tevatron [18]. The dilution factors for s, c, and b quarks are very close to 0.5 [8–10], and thus the s, c, and b quark contributions are significantly suppressed. As a result, P_u and P_d at the Tevatron are approximately

$$\begin{aligned} P_u &\sim u(x_1)u(x_2)/\sigma_{\rm total}(x_1,x_2), \\ P_d &\sim d(x_1)d(x_2)/\sigma_{\rm total}(x_1,x_2), \end{aligned} \tag{4}$$

where $x_{1,2}$ are the Bjorken variables for the colliding quark and antiquark, respectively, defined at leading order as $x_{1,2} = \frac{\sqrt{M^2+Q_T^2}}{\sqrt{s}} e^{\pm Y}$. The ratio $R = P_u/P_d$, in which the total cross section cancels, represents the relative contribution of u and d quarks. Owing to the detector acceptance discussed below, the data in this measurement have dilepton rapidity in the interval $|Y| = [0, 2.3]$. The P_u, P_d, and R measured in this paper correspond to the values of x from approximately 0.004 to 0.45. We obtain information on the x dependence of the structure parameters by analyzing the data separately for $|Y|$ intervals of [0, 0.5], [0.5, 1.0], [1.0, 1.5], and [1.5, 2.3]. The ranges of the x_1 and x_2 values for different $|Y|$ bins have small overlaps due to the preponderance of data in the small mass interval around the Z boson pole.

The D0 detector consists of tracking detectors surrounded by a solenoid magnet, calorimeters, and a muon system [19–21]. Dielectron and dimuon events are collected with lepton triggers and are required to have a lepton-antilepton pair in the offline analysis. Leptons are required to be well separated from other particles in both the tracking system and the calorimeter. Muons are measured as tracks in the tracking and muon detectors with $|\eta_{\rm det}| < 1.8$ [22], and are required to have transverse momentum $p_T > 15$ GeV. Electrons are reconstructed as clusters in the central calorimeter with $|\eta_{\rm det}| < 1.1$, and in an end calorimeter (EC) with $1.5 < |\eta_{\rm det}| < 3.5$. They are required to have a spatially matched track in the tracking system so that their electric charge can be determined, and for discriminating against photons. The threshold for the electron p_T is 25 GeV. The EC-EC events, where both electrons are in an EC, are excluded due to the higher level of background for such events. As a result, the background contributions from $Z/\gamma^* \to \tau\tau$, W + jets, diboson (WW and WZ), $\gamma\gamma$, top quarks, and multijets are suppressed

to $\mathcal{O}(1\%)$ in the mass region $70 < M < 116$ GeV used in this analysis.

A Monte Carlo (MC) sample of $Z/\gamma^* \to \ell^+\ell^-$ events is generated using the leading-order PYTHIA generator [23] with CT18NNLO PDFs, followed by a Geant-based [24] simulation of the D0 detector. The samples are further corrected by reweighting the MC events at the generator level in M, Q_T, Y, and $\cos\theta$ to match the calculation of ResBos [17], which is at the approximate next-to-next-to-leading order and next-to-next-to-leading logarithm in QCD. The electron energy and muon momentum are calibrated using the known resonances in the dilepton mass spectrum. The efficiencies of the online and offline selection criteria are determined using the tag-and-probe method [25] and the MC simulation is corrected to be consistent with the data. The multijets background is estimated using data, while other backgrounds are determined using the PYTHIA MC simulations. The methodologies used to derive the energy and momentum calibrations, efficiencies, and estimates of the background contributions were also employed in the previous measurements of the effective weak mixing angle [26,27]. Many systematic effects are suppressed since A_{FB} is defined as a ratio. The observed A_{FB} distributions as a function of M in different intervals are shown in Fig. 2 with comparisons to the corresponding predictions from the simulated MC samples.

For the measurement of P_u and P_d in the full $0 < |Y| < 2.3$ range, or in a particular $|Y|$ interval, a set of MC template distributions of A_{FB} is prepared in which P_u and P_d are varied while keeping Δ_u and Δ_d fixed at their values calculated using ResBos and CT18NNLO. A set of $\mathcal{C}_q = P_q + \Delta_q$ values is calculated for intervals in Y, M, and Q_T [28]. A_{FB} templates are acquired by reweighting the generator-level differential cross sections $\sigma_q(Y, M, Q_T, \cos\theta)$ of the MC sample according to the $\mathcal{C}_q$ value. In the MC reweighting procedures, A_{FB}^u and A_{FB}^d are calculated using ResBos, with $\sin^2\theta_{\rm eff}^\ell$ set to the average of the results from the electron-positron colliders LEP and SLC [29]. The uncertainties on $\sin^2\theta_{\rm eff}^\ell$ are propagated to the measured P_u and P_d. We do not use the hadron collider results on $\sin^2\theta_{\rm eff}^\ell$, in order to avoid the influence from the specific PDF predictions used in their measurement, but this choice has a negligible impact on the result because the hadron collider measurements [30–33] give values of $\sin^2\theta_{\rm eff}^\ell$ very close to the combined LEP/SLC result. Uncertainties on Δ_u and Δ_d are estimated using the error PDF sets given by CT18NNLO. The differences in Δ_u and Δ_d for different PDF sets are well covered by the estimated uncertainty. Equation (2) is strictly true only when Y and Q_T dependences are fully considered. In this paper, the observed A_{FB} is averaged over Q_T and Y intervals so that the factorization formalism of Eq. (2) becomes an approximation. This gives rise to additional uncertainties in the calculation of σ_q and higher-order QCD contributions. Part of this uncertainty is already included when taking the CT18NNLO error PDF sets into account. The remainder is estimated by varying the Q_T distribution of ResBos to match the predictions of PYTHIA.

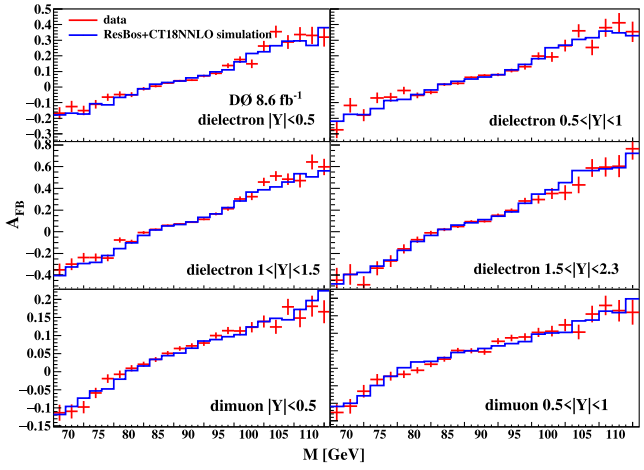

FIG. 2. A_{FB} distribution as a function of M in different Y bins observed from data compared to the corresponding predictions from the simulated MC samples. The P_u and P_d parameters in the MC samples have the fitted values listed in Table II.

P_u and P_d are determined by requiring the best agreement between the observed A_{FB} distributions in both the dielectron and dimuon events and their corresponding MC templates. Since P_u and P_d are simultaneously fitted, their values and corresponding uncertainties are correlated with a correlation coefficient $\rho = -0.859$. The central value of R and its uncertainty are calculated using the measured values and the total uncertainties of P_u and P_d, and their correlation.

The measured P_u, P_d, and the ratio R in the full range $|Y| = [0, 2.3]$ are

$$\begin{aligned} P_u &= 0.602 \pm 0.019(\text{stat}) \pm 0.010(\text{theory}) \pm 0.006(\text{syst}) \\ &= 0.602 \pm 0.022, \\ P_d &= 0.258 \pm 0.023(\text{stat}) \pm 0.012(\text{theory}) \pm 0.005(\text{syst}) \\ &= 0.258 \pm 0.026, \\ R &= 2.34 \pm 0.32. \end{aligned}$$

The systematic uncertainty corresponds to the quadratic sum of the uncertainties of efficiency determination, lepton calibration, and background estimation. The theory uncertainty is the quadratic sum of the uncertainties due to the Δ parameters, QCD calculation, and value of $\sin^2\theta_{\rm eff}^\ell$. The systematic and theoretical uncertainties are small compared to the statistical uncertainties. Compared to the predictions of CT18NNLO, MSHT20 [9], and NNPDF4.0 [10] shown in Table I, the measured P_u is lower than the PDF predictions, while P_d is higher. The ratio R is lower than the predictions by about 2 standard deviations (the largest

TABLE I. Measured values of P_u, P_d, and R in the full $|Y|$ range [0, 2.3], together with their predictions from the CT18NNLO, MSHT20, and NNPDF4.0 PDFs. The predictions are calculated using ResBos based on the definition in Eqs. (2) and (3). The measured values are presented with their total uncertainties. The theoretical predictions are calculated in the same $|Y|$ range and shown with their PDF uncertainties.

	P_u	P_d	R
Measured	0.602 ± 0.022	0.258 ± 0.026	2.34 ± 0.32
CT18NNLO	0.636 ± 0.011	0.213 ± 0.009	2.99 ± 0.16
MSHT20	0.633 ± 0.009	0.204 ± 0.008	3.10 ± 0.14
NNPDF4.0	0.624 ± 0.008	0.190 ± 0.007	3.29 ± 0.13

TABLE II. Measurements of P_u, P_d, and R in different $|Y|$ bins. The uncertainties, in order, are statistical, experimental systematic, Δ-induced, $\sin^2\theta^{\ell}_{\rm eff}$, and QCD modeling. The final column is the total uncertainty.

$\lvert Y\rvert$ range	P_u	δP_u
[0, 0.5]	$0.515 \pm 0.031 \pm 0.011 \pm 0.009 \pm 0.004 \pm 0.005$	0.034
[0.5, 1.0]	$0.589 \pm 0.035 \pm 0.010 \pm 0.008 \pm 0.004 \pm 0.005$	0.038
[1.0, 1.5]	$0.568 \pm 0.036 \pm 0.007 \pm 0.010 \pm 0.005 \pm 0.003$	0.038
[1.5, 2.3]	$0.680 \pm 0.060 \pm 0.009 \pm 0.020 \pm 0.005 \pm 0.003$	0.064

$\lvert Y\rvert$ range	P_d	δP_d
[0, 0.5]	$0.232 \pm 0.036 \pm 0.007 \pm 0.007 \pm 0.008 \pm 0.001$	0.038
[0.5, 1.0]	$0.189 \pm 0.042 \pm 0.008 \pm 0.007 \pm 0.008 \pm 0.004$	0.044
[1.0, 1.5]	$0.348 \pm 0.046 \pm 0.005 \pm 0.008 \pm 0.010 \pm 0.002$	0.048
[1.5, 2.3]	$0.252 \pm 0.076 \pm 0.014 \pm 0.020 \pm 0.009 \pm 0.002$	0.081

$\lvert Y\rvert$ range	R	δR
[0, 0.5]	2.22	0.50
[0.5, 1.0]	3.11	0.90
[1.0, 1.5]	1.63	0.33
[1.5, 2.3]	2.70	1.09

difference, 2.8 standard deviations, is observed for NNPDF4.0).

The $|Y|$-dependent measurements using both the dielectron and dimuon A_{FB} distributions are shown in Table II. The correlation coefficients of P_u and P_d in the four $|Y|$ intervals are −0.855, −0.862, −0.866, and −0.871, respectively. The comparison between the measured values and the predictions from representative PDFs is shown in Fig. 3. For $1 < |Y| < 1.5$, the measured R differs from the PDF predictions by about 3.5 standard deviations, suggesting that the d quark contribution is higher than the PDF expectations. This interval corresponds to $x \sim 0.2$ for the quark with higher energy and $x \sim 0.01$ for the quark with lower energy, covering the peak of the parton density distributions of the u and d quarks. For the other three bins, the measurements of P_u and P_d show good agreement with the predictions. In Fig. 4, we show the pull of A_{FB}, which is

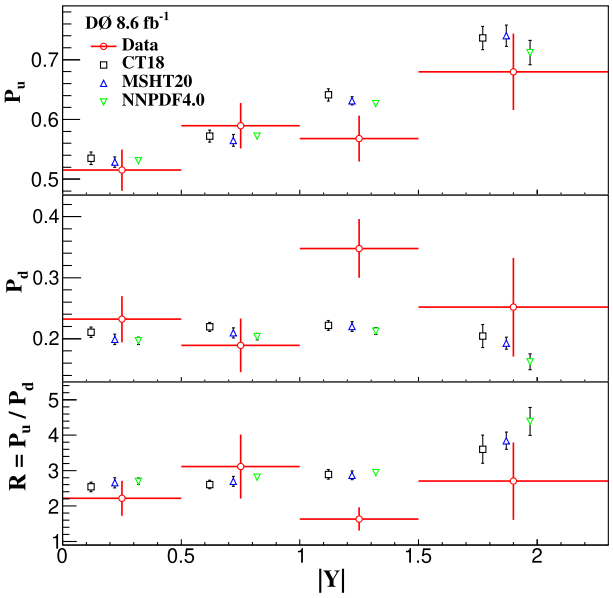

FIG. 3. Measured values of P_u, P_d, and R parameters compared with the predictions of CT18NNLO, MSHT20, and NNPDF4.0. Error bars of the data points correspond to the total uncertainty of the measurement, while error bars on the predictions correspond to the PDF uncertainties. The PDF predictions are offset from the centers of the intervals for clarity.

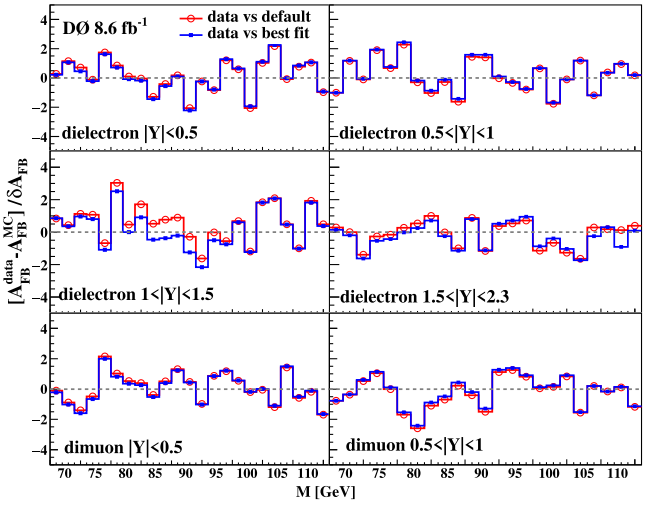

FIG. 4. The pull of A_{FB} distribution, calculated using the A_{FB} predictions corresponding to the default P_u and P_d values in CT18NNLO predictions, and using the predictions corresponding to the best fitted values of P_u and P_d.

defined as the difference between the measured A_{FB} value and the predicted A_{FB} value divided by the uncertainty of the measured A_{FB}. The pulls of the best fit P_u and P_d values shown in Fig. 4 conform well to the expected distributions.

The measurements of P_u and P_d for dielectron and dimuon channels separately are given in Table III. Owing to the limited detector acceptance and efficiencies for the

TABLE III. Central values and uncertainties of the $|Y|$-dependent P_u and P_d parameters using dielectron events and dimuon events. The uncertainties, in order, are statistical, experimental systematics, and theoretical systematics including PDF, $\sin^2\theta^{\ell}_{\rm eff}$, and QCD modeling. The last column, δP_q, gives the total uncertainty. The predictions for CT18NNLO are shown with the corresponding PDF uncertainties.

$\lvert Y\rvert$ range		P_u	δP_u
[0, 0.5]	ee	$0.554 \pm 0.048 \pm 0.008 \pm 0.010$	0.049
	$\mu\mu$	$0.504 \pm 0.041 \pm 0.017 \pm 0.014$	0.047
	CT18NNLO	0.535 ± 0.010	
[0.5, 1]	ee	$0.528 \pm 0.049 \pm 0.010 \pm 0.010$	0.051
	$\mu\mu$	$0.656 \pm 0.054 \pm 0.017 \pm 0.013$	0.058
	CT18NNLO	0.572 ± 0.010	

$\lvert Y\rvert$ range		P_d	δP_d
[0, 0.5]	ee	$0.143 \pm 0.063 \pm 0.004 \pm 0.010$	0.064
	$\mu\mu$	$0.266 \pm 0.044 \pm 0.012 \pm 0.012$	0.047
	CT18NNLO	0.211 ± 0.008	
[0.5, 1]	ee	$0.270 \pm 0.066 \pm 0.007 \pm 0.011$	0.067
	$\mu\mu$	$0.124 \pm 0.055 \pm 0.013 \pm 0.012$	0.058
	CT18NNLO	0.220 ± 0.007	

muons, the dimuon events contribute appreciably only to the two lower $|Y|$ intervals. For both the P_u and P_d parameters in the two lower $|Y|$ bins, the electron and muon measurements agree within 1.7 standard deviations.

The precision in this analysis is better than the previous DIS measurements that provide indirect constraints on the d quark density. For example, the ν-Fe measurement gives a relative uncertainty larger than 25% [12], while the relative uncertainty on P_u and P_d is about 10% in this analysis. In addition, P_u and P_d have higher sensitivity to the valence quarks due to the quadratic terms in Eq. (4). A previous study [34] used asymmetries that were deconvoluted from the measured values to remove the effects of the detector resolution, unlike the current analysis, which uses the measured asymmetries directly. Such unfolding depends significantly upon the PDF predictions, and thus contains assumptions about the u and d quark densities that are being studied. In the current analysis, the P_u and P_d parameters are measured by comparing the uncorrected data and simulated MC events, and hence there is no unfolding-related bias.

In conclusion, we have performed a new measurement of the proton structure parameters P_u and P_d using $p\bar{p} \to Z/\gamma^* \to \ell^+\ell^-$ events of Tevatron data corresponding to 8.6 fb^{-1} of integrated luminosity. Taking advantage of the asymmetry of the weak interaction, the u and d quark contributions are determined separately, giving a model-independent measurement of the valence d quarks. For $p\bar{p}$ collisions at $\sqrt{s} = 1.96$ TeV, P_u and P_d are dominated by the valence u and d quarks for $0.004 < x < 0.45$. P_u, P_d, and their ratio R are measured both for the dilepton rapidity interval $|Y| = [0, 2.3]$ and for finer $|Y|$ intervals to investigate their dependence on x. The ratio of P_u and P_d is consistent with the CT18NNLO, MSHT20, and NNPDF4.0 PDF predictions for dilepton rapidities less than 1. However, for the interval $1 < |Y| < 1.5$, it is smaller than predicted for the PDFs by a factor of between 3.5 and 3.7 standard deviations. For this interval, the x value of the quark with the larger Bjorken x is near the peak of the valence quark distribution, while that of the smaller x quark is about 0.01.

This document was prepared by the D0 Collaboration using the resources of the Fermi National Accelerator Laboratory (Fermilab), a U.S. Department of Energy, Office of Science, HEP User Facility. Fermilab is managed by Fermi Research Alliance, LLC (FRA), acting under Contract No. DE-AC02-07CH11359. We thank the staffs at Fermilab and collaborating institutions and acknowledge support from the Department of Energy and the National Science Foundation (U.S.); the Alternative Energies and Atomic Energy Commission and the National Center for Scientific Research/National Institute of Nuclear and Particle Physics (France); the Ministry of Education and Science of the Russian Federation, the National Research Center "Kurchatov Institute" of the Russian Federation, and the Russian Foundation for Basic Research (Russia); National Council for the Development of Science and Technology and Carlos Chagas Filho Foundation for the Support of Research in the State of Rio de Janeiro (Brazil); the Department of Atomic Energy and Department of Science and Technology (India); the Administrative Department of Science, Technology and Innovation (Colombia); the National Council of Science and Technology (Mexico); the National Research Foundation of Korea (Korea); the Foundation for Fundamental Research on Matter (The Netherlands); the Science and Technology Facilities Council and The Royal Society (United Kingdom); the Ministry of Education, Youth and Sports (Czech Republic); Bundesministerium für Bildung und Forschung (Federal Ministry of Education and Research) and Deutsche Forschungsgemeinschaft (German Research Foundation; Germany); Science Foundation Ireland (Ireland); the Swedish Research Council (Sweden); and China Academy of Sciences and National Natural Science Foundation of China (China).

[1] H. Abramowicz *et al.* (H1 and ZEUS Collaborations), Combination of measurements of inclusive deep inelastic $e^{\pm}p$ scattering cross sections and QCD analysis of HERA data, Eur. Phys. J. C **75**, 580 (2015).

[2] A. C. Benvenuti *et al.* (BCDMS Collaboration), A high statistics measurement of the proton structure functions $F_2(x, Q^2)$ and R from deep inelastic muon scattering at high Q^2, Phys. Lett. B **223**, 485 (1989).

[3] A. C. Benvenuti *et al.* (BCDMS Collaboration), A high statistics measurement of the deuteron structure functions $F_2(x, Q^2)$ and R from deep inelastic muon scattering at high Q^2, Phys. Lett. B **237**, 592 (1990).

[4] M. Arneodo *et al.* (New Muon Collaboration), Measurement of the proton and deuteron structure functions, F_2^p and F_2^d, and of the ratio σ_L/σ_T, Nucl. Phys. **B483**, 3 (1997).

[5] G. Moreno *et al.*, Dimuon production in proton-copper collisions at $\sqrt{s} = 38.8$ GeV, Phys. Rev. D **43**, 2815 (1991).

[6] R. S. Towell *et al.* (NuSea Collaboration), Improved measurement of the $\bar{d}/\bar{u}$ asymmetry in the nucleon sea, Phys. Rev. D **64**, 052002 (2001).

[7] J. C. Webb *et al.* (NuSea Collaboration), Measurement of the absolute Drell-Yan dimuon cross sections in 800 GeV/c pp and pd collisions, Nucl. Phys. **A721**, C344 (2003).

[8] Tie-Jiun Hou, Jun Gao, T. J. Hobbs *et al.*, New CTEQ global analysis of quantum chromodynamics with high precision data from the LHC, Phys. Rev. D **103**, 014013 (2021).

[9] S. Bailey, T. Cridge, L. A. Harland-Lang, A. D. Martin, and R. S. Thorne, Parton distributions from LHC, HERA, Tevatron and fixed target data: MSHT20 PDFs, Eur. Phys. J. C **81**, 341 (2021).

[10] R. D. Ball *et al.* (NNPDF Collaboration), The path to proton structure at 1% accuracy, Eur. Phys. J. C **82**, 428 (2022).

[11] J. P. Berge *et al.*, A measurement of differential cross-sections and nucleon structure functions in charged-current neutrino interactions on iron, Z. Phys. C **49**, 187 (1991).

[12] W. G. Seligman *et al.* (CCFR Collaboration), Improved determination of α_s from neutrino-nucleon scattering, Phys. Rev. Lett. **79**, 1213 (1997).

[13] H. Abramowicz *et al.* (H1 and ZEUS Collaborations), Inclusive deep inelastic scattering at high Q^2 with longitudinally polarised beams at HERA, J. High Energy Phys. 09 (2012) 061.

[14] Siqi Yang, Yao Fu, Minghui Liu, Liang Han, Tie-Jiun Hou, and C.-P. Yuan, Factorization of the forward-backward asymmetry and measurements of the weak mixing angle and proton structure at hadron colliders, Phys. Rev. D **106**, 033001 (2022).

[15] Siqi Yang, Yao Fu, Minghui Liu, Renyou Zhang, Tie-Jiun Hou, Chen Wang, Hang Yin, Liang Han, and C.-P. Yuan, Reduction of the electroweak correlation in the PDF updating by using the forward-backward asymmetry of Drell-Yan process, Eur. Phys. J. C **82**, 368 (2022).

[16] J. C. Collins and D. E. Soper, Angular distribution of dileptons in high-energy hadron collisions, Phys. Rev. D **16**, 2219 (1977).

[17] C. Balazs and C. P. Yuan, Soft gluon effects on lepton pairs at hadron colliders, Phys. Rev. D **56**, 5558 (1997).

[18] The dilution factors for $u\bar{u}$ and $d\bar{d}$ subprocesses are less than 10% and 20%, respectively.

[19] V. M. Abazov *et al.* (D0 Collaboration), The upgraded D0 detector, Nucl. Instrum. Methods Phys. Res., Sect. A **565**, 463 (2006).

[20] V. M. Abazov *et al.* (D0 Collaboration), Design and implementation of the new D0 level-1 calorimeter trigger, Nucl. Instrum. Methods Phys. Res., Sect. A **584**, 75 (2008).

[21] V. M. Abazov *et al.* (D0 Collaboration), The layer-0 inner silicon detector of the D0 experiment, Nucl. Instrum. Methods Phys. Res., Sect. A **622**, 298 (2010).

[22] We use a cylindrical coordinate system with the z axis along the proton beam direction. Pseudorapidity is defined as $\eta = -\ln[\tan(\theta_{\rm pol}/2)]$, where the polar angle $\theta_{\rm pol}$ is measured with respect to the interaction vertex. In the massless limit, η is equivalent to the rapidity $y = (1/2)\ln[(E + p_z)/(E - p_z)]$, and $\eta_{\rm det}$ is the pseudorapidity measured with respect to the center of the detector.

[23] T. Sjöstrand, P. Edén, C. Feriberg, L. Lönnblad, G. Miu, S. Mrenna, and E. Norrbin, High-energy-physics event generation with PYTHIA 6.1, Comput. Phys. Commun. **135**, 238 (2001).

[24] R. Brun and F. Carminati, Geant detector description and simulation tool, CERN program library long write-up W5013 (unpublished).

[25] V. M. Abazov *et al.* (D0 Collaboration), Measurement of the shape of the boson rapidity distribution for $p\bar{p} \to Z/\gamma^* \to e^+e^- + X$ events produced at $\sqrt{s} = 1.96$ TeV, Phys. Rev. D **76**, 012003 (2007).

[26] V. M. Abazov *et al.* (D0 Collaboration), Measurement of the effective weak mixing angle in $p\bar{p} \to Z/\gamma^* \to e^+e^-$ events, Phys. Rev. Lett. **115**, 041801 (2015).

[27] V. M. Abazov *et al.* (D0 Collaboration), Measurement of the effective weak mixing angle in $p\bar{p} \to Z/\gamma^* \to \ell^+\ell^-$ events, Phys. Rev. Lett. **120**, 241802 (2018).

[28] We use a bin size of 1 GeV for the M dependence and a bin size of 0.1 for the Y dependence. For the Q_T dependence, the bin size is 1, 10, and 100 GeV for $Q_T < 10$, $10 < Q_T < 50$, and $50 < Q_T < 250$ GeV, respectively.

[29] G. Abbiendi *et al.* (LEP, ALEPH, DELPHI, L3 and OPAL Collaborations, SLD, LEP Electronweak Working, SLD Electroweak, and Heavy Flavor Groups), Precision electroweak measurements on the Z resonance, Phys. Rep. **427**, 257 (2006).

[30] T. Aaltonen *et al.* (CDF and D0 Collaborations), Tevatron Run II combination of the effective leptonic electroweak mixing angle, Phys. Rev. D **97**, 112007 (2018).

[31] See the ATLAS public note at https://atlas.web.cern.ch/Atlas/GROUPS/PHYSICS/CONFNOTES/ATLAS-CONF-2018-037/.

[32] A. M. Sirunyan *et al.* (CMS Collaboration), Measurement of the weak mixing angle using the forward-backward asymmetry of Drell-Yan events in pp collisions at 8 TeV, Eur. Phys. J. C **78**, 701 (2018).

[33] R. Aaij *et al.* (LHCb Collaboration), Measurement of the forward-backward asymmetry in $Z/\gamma^* \to \mu^+\mu^-$ decays and determination of the effective weak mixing angle, J. High Energy Phys. 11 (2015) 190.

[34] Mingzhe Xie, Siqi Yang, Yao Fu, Minghui Liu, Liang Han, Tie-Juin Hou, Sayipjamal Dulat, and C.-P. Yuan, Measurement of the proton structure parameters in the forward-backward charge asymmetry, Phys. Rev. D **107**, 054008 (2023).

V. M. Abazov,[31] B. Abbott,[66] B. S. Acharya,[25] M. Adams,[45] T. Adams,[43] J. P. Agnew,[40] G. D. Alexeev,[31] G. Alkhazov,[35] A. Alton,[55,b] A. Askew,[43] S. Atkins,[53] K. Augsten,[7] C. Avila,[5] F. Badaud,[10] L. Bagby,[44] B. Baldin,[44] D. V. Bandurin,[73] S. Banerjee,[25] E. Barberis,[54] P. Baringer,[52] J. F. Bartlett,[44] U. Bassler,[15] V. Bazterra,[45] A. Bean,[52] M. Begalli,[2] L. Bellantoni,[44] S. B. Beri,[23] G. Bernardi,[14] R. Bernhard,[19] I. Bertram,[38] M. Besançon,[15] R. Beuselinck,[39] P. C. Bhat,[44] S. Bhatia,[57] V. Bhatnagar,[23] G. Blazey,[46] S. Blessing,[43] K. Bloom,[58] A. Boehnlein,[44] D. Boline,[63] E. E. Boos,[33] G. Borissov,[38] A. Brandt,[70] O. Brandt,[20] M. Brochmann,[74] R. Brock,[56] A. Bross,[44] D. Brown,[14] X. B. Bu,[44] M. Buehler,[44] V. Buescher,[21] V. Bunichev,[33] S. Burdin,[38,c] C. P. Buszello,[37] E. Camacho-Pérez,[28] B. C. K. Casey,[44] H. Castilla-Valdez,[28] S. Caughron,[56] S. Chakrabarti,[63] K. M. Chan,[50] A. Chandra,[72] E. Chapon,[15] G. Chen,[52] S. W. Cho,[27] S. Choi,[27] B. Choudhary,[24] S. Cihangir,[44,a] D. Claes,[58] J. Clutter,[52] M. Cooke,[44,k] W. E. Cooper,[44] M. Corcoran,[72,a] F. Couderc,[15] M.-C. Cousinou,[12] J. Cuth,[21] D. Cutts,[69] A. Das,[71] G. Davies,[39] S. J. de Jong,[29,30] E. De La Cruz-Burelo,[28] F. Déliot,[15] R. Demina,[62] D. Denisov,[64] S. P. Denisov,[34] S. Desai,[44] C. Deterre,[40,d] K. DeVaughan,[58] H. T. Diehl,[44] M. Diesburg,[44] P. F. Ding,[40] A. Dominguez,[58] A. Drutskoy,[32,p] A. Dubey,[24] L. V. Dudko,[33] A. Duperrin,[12] S. Dutt,[23] M. Eads,[46] D. Edmunds,[56] J. Ellison,[42] V. D. Elvira,[44] Y. Enari,[14] H. Evans,[48] A. Evdokimov,[45] V. N. Evdokimov,[34] A. Fauré,[15] L. Feng,[46] T. Ferbel,[62,a] F. Fiedler,[21] F. Filthaut,[29,30] W. Fisher,[56] H. E. Fisk,[44,a] M. Fortner,[46] H. Fox,[38] J. Franc,[7] S. Fuess,[44] P. H. Garbincius,[44] A. Garcia-Bellido,[62] J. A. García-González,[28] V. Gavrilov,[32] W. Geng,[12,56] C. E. Gerber,[45] Y. Gershtein,[59] G. Ginther,[44] G. Golovanov,[31,a] P. D. Grannis,[63] S. Greder,[16] H. Greenlee,[44] G. Grenier,[17] Ph. Gris,[10] J.-F. Grivaz,[13] A. Grohsjean,[15,d] S. Grünendahl,[44] M. W. Grünewald,[26] T. Guillemin,[13] G. Gutierrez,[44] P. Gutierrez,[66] J. Haley,[67] L. Han,[4] K. Harder,[40] A. Harel,[62] J. M. Hauptman,[51] J. Hays,[39] T. Head,[40] T. Hebbeker,[18] D. Hedin,[46] H. Hegab,[67] A. P. Heinson,[42] U. Heintz,[69] C. Hensel,[1] I. Heredia-De La Cruz,[28,e] K. Herner,[44] G. Hesketh,[40,g] M. D. Hildreth,[50] R. Hirosky,[73] T. Hoang,[43] J. D. Hobbs,[63] B. Hoeneisen,[9] J. Hogan,[72] M. Hohlfeld,[21] J. L. Holzbauer,[57] I. Howley,[70] Z. Hubacek,[7,15] V. Hynek,[7] I. Iashvili,[61] Y. Ilchenko,[71] R. Illingworth,[44] A. S. Ito,[44] S. Jabeen,[44,l] M. Jaffré,[13] A. Jayasinghe,[66] M. S. Jeong,[27] R. Jesik,[39] P. Jiang,[4,a] K. Johns,[41] E. Johnson,[56] M. Johnson,[44] A. Jonckheere,[44] P. Jonsson,[39] J. Joshi,[42] A. W. Jung,[44,o] A. Juste,[36] E. Kajfasz,[12] D. Karmanov,[33] I. Katsanos,[58] M. Kaur,[23] R. Kehoe,[71] S. Kermiche,[12] N. Khalatyan,[44] A. Khanov,[67] A. Kharchilava,[61] Y. N. Kharzheev,[31] I. Kiselevich,[32] J. M. Kohli,[23] A. V. Kozelov,[34,a] J. Kraus,[57] A. Kumar,[61] A. Kupco,[8] T. Kurča,[17] V. A. Kuzmin,[33] S. Lammers,[48] P. Lebrun,[17] H. S. Lee,[27] S. W. Lee,[51] W. M. Lee,[44,a] X. Lei,[41] J. Lellouch,[14] D. Li,[14] H. Li,[73] L. Li,[42] Q. Z. Li,[44] J. K. Lim,[27] D. Lincoln,[44] J. Linnemann,[56] V. V. Lipaev,[34,a] R. Lipton,[44] H. Liu,[71] Y. Liu,[4] A. Lobodenko,[35] M. Lokajicek,[8,a] R. Lopes de Sa,[44] R. Luna-Garcia,[28,h] A. L. Lyon,[44] A. K. A. Maciel,[1] R. Madar,[19] R. Magaña-Villalba,[28] S. Malik,[58] V. L. Malyshev,[31] J. Mansour,[20] J. Martínez-Ortega,[28] R. McCarthy,[63] C. L. McGivern,[40] M. M. Meijer,[29,30] A. Melnitchouk,[44] D. Menezes,[46] P. G. Mercadante,[3] M. Merkin,[33] A. Meyer,[18] J. Meyer,[20,j] F. Miconi,[16] N. K. Mondal,[25] M. Mulhearn,[73] E. Nagy,[12] M. Narain,[69,a] R. Nayyar,[41] H. A. Neal,[55,a] J. P. Negret,[5] P. Neustroev,[35] H. T. Nguyen,[73] T. Nunnemann,[22] J. Orduna,[69] N. Osman,[12] A. Pal,[70] N. Parashar,[49] V. Parihar,[69] S. K. Park,[27] R. Partridge,[69,f] N. Parua,[48] A. Patwa,[64,k] B. Penning,[39] M. Perfilov,[33] Y. Peters,[40] K. Petridis,[40] G. Petrillo,[62] P. Pétroff,[13] M.-A. Pleier,[64] V. M. Podstavkov,[44] A. V. Popov,[34] M. Prewitt,[72] D. Price,[40] N. Prokopenko,[34] J. Qian,[55] A. Quadt,[20] B. Quinn,[57] P. N. Ratoff,[38] I. Razumov,[60] I. Ripp-Baudot,[16] F. Rizatdinova,[67] M. Rominsky,[44] A. Ross,[38] C. Royon,[52] P. Rubinov,[44] R. Ruchti,[50] G. Sajot,[11] A. Sánchez-Hernández,[28] M. P. Sanders,[22] A. S. Santos,[1,i] G. Savage,[44] L. Sawyer,[53] T. Scanlon,[39] R. D. Schamberger,[63] Y. Scheglov,[35,a] H. Schellman,[68,47] M. Schott,[21] C. Schwanenberger,[40,d] R. Schwienhorst,[56] J. Sekaric,[52] H. Severini,[66] E. Shabalina,[20] V. Shary,[15] S. Shaw,[40] A. A. Shchukin,[34] V. Simak,[7,a] P. Skubic,[66] P. Slattery,[62] G. R. Snow,[58,a] J. Snow,[65] S. Snyder,[64] S. Söldner-Rembold,[40] L. Sonnenschein,[18] K. Soustruznik,[6] J. Stark,[11] D. A. Stoyanova,[34] M. Strauss,[66] L. Suter,[40] P. Svoisky,[73] M. Titov,[15] V. V. Tokmenin,[31,a] Y.-T. Tsai,[62] D. Tsybychev,[63] B. Tuchming,[15] C. Tully,[60] L. Uvarov,[35] S. Uvarov,[35] S. Uzunyan,[46] R. Van Kooten,[48] W. M. van Leeuwen,[29] N. Varelas,[45] E. W. Varnes,[41] I. A. Vasilyev,[34] A. Y. Verkheev,[31] L. S. Vertogradov,[31] M. Verzocchi,[44] M. Vesterinen,[40] D. Vilanova,[15] P. Vokac,[7] H. D. Wahl,[43,a] C. Wang,[4] M. H. L. S. Wang,[44] J. Warchol,[50,a] G. Watts,[74]

M. Wayne,[50] J. Weichert,[21] L. Welty-Rieger,[47] M. R. J. Williams,[48,m] G. W. Wilson,[52] M. Wobisch,[53] D. R. Wood,[54] T. R. Wyatt,[40] M. Xie,[4] Y. Xie,[44] R. Yamada,[44,a] S. Yang,[4] T. Yasuda,[44] Y. A. Yatsunenko,[31,a] W. Ye,[63] Z. Ye,[44] H. Yin,[44] K. Yip,[64] S. W. Youn,[44] J. M. Yu,[55] J. Zennamo,[61] T. G. Zhao,[40] B. Zhou,[55] J. Zhu,[55] M. Zielinski,[62] D. Zieminska,[48] and L. Zivkovic[14,o]

(D0 Collaboration)

[1]*LAFEX, Centro Brasileiro de Pesquisas Físicas, Rio de Janeiro, Rio de Janeiro 22290, Brazil*
[2]*Universidade do Estado do Rio de Janeiro, Rio de Janeiro, Rio de Janeiro 20550, Brazil*
[3]*Universidade Federal do ABC, Santo André, São Paulo 09210, Brazil*
[4]*University of Science and Technology of China, Hefei 230026, People's Republic of China*
[5]*Universidad de los Andes, Bogotá 111711, Colombia*
[6]*Charles University, Faculty of Mathematics and Physics, Center for Particle Physics, 116 36 Prague 1, Czech Republic*
[7]*Czech Technical University in Prague, 116 36 Prague 6, Czech Republic*
[8]*Institute of Physics, Academy of Sciences of the Czech Republic, 182 21 Prague, Czech Republic*
[9]*Universidad San Francisco de Quito, Quito 170157, Ecuador*
[10]*LPC, Université Blaise Pascal, CNRS/IN2P3, Clermont, F-63178 Aubière Cedex, France*
[11]*LPSC, Université Joseph Fourier Grenoble 1, CNRS/IN2P3, Institut National Polytechnique de Grenoble, F-38026 Grenoble Cedex, France*
[12]*CPPM, Aix-Marseille Université, CNRS/IN2P3, F-13288 Marseille Cedex 09, France*
[13]*LAL, Université Paris-Sud, CNRS/IN2P3, Université Paris-Saclay, F-91898 Orsay Cedex, France*
[14]*LPNHE, Universités Paris VI and VII, CNRS/IN2P3, F-75005 Paris, France*
[15]*IRFU, CEA, Université Paris-Saclay, F-91191 Gif-Sur-Yvette, France*
[16]*IPHC, Université de Strasbourg, CNRS/IN2P3, F-67037 Strasbourg, France*
[17]*IPNL, Université Lyon 1, CNRS/IN2P3, F-69622 Villeurbanne Cedex, France and Université de Lyon, F-69361 Lyon CEDEX 07, France*
[18]*III. Physikalisches Institut A, RWTH Aachen University, 52056 Aachen, Germany*
[19]*Physikalisches Institut, Universität Freiburg, 79085 Freiburg, Germany*
[20]*II. Physikalisches Institut, Georg-August-Universität Göttingen, 37073 Göttingen, Germany*
[21]*Institut für Physik, Universität Mainz, 55099 Mainz, Germany*
[22]*Ludwig-Maximilians-Universität München, 80539 München, Germany*
[23]*Panjab University, Chandigarh 160014, India*
[24]*Delhi University, Delhi-110 007, India*
[25]*Tata Institute of Fundamental Research, Mumbai-400 005, India*
[26]*University College Dublin, Dublin 4, Ireland*
[27]*Korea Detector Laboratory, Korea University, Seoul 02841, Korea*
[28]*CINVESTAV, Mexico City 07360, Mexico*
[29]*Nikhef, Science Park, 1098 XG Amsterdam, The Netherlands*
[30]*Radboud University Nijmegen, 6525 AJ Nijmegen, The Netherlands*
[31]*Joint Institute for Nuclear Research, Dubna 141980, Russia*
[32]*Institute for Theoretical and Experimental Physics, Moscow 117259, Russia*
[33]*Moscow State University, Moscow 119991, Russia*
[34]*Institute for High Energy Physics, Protvino, Moscow Region 142281, Russia*
[35]*Petersburg Nuclear Physics Institute, St. Petersburg 188300, Russia*
[36]*Institució Catalana de Recerca i Estudis Avançats (ICREA) and Institut de Física d'Altes Energies (IFAE), 08193 Bellaterra (Barcelona), Spain*
[37]*Uppsala University, 751 05 Uppsala, Sweden*
[38]*Lancaster University, Lancaster LA1 4YB, United Kingdom*
[39]*Imperial College London, London SW7 2AZ, United Kingdom*
[40]*The University of Manchester, Manchester M13 9PL, United Kingdom*
[41]*University of Arizona, Tucson, Arizona 85721, USA*
[42]*University of California Riverside, Riverside, California 92521, USA*
[43]*Florida State University, Tallahassee, Florida 32306, USA*
[44]*Fermi National Accelerator Laboratory, Batavia, Illinois 60510, USA*
[45]*University of Illinois at Chicago, Chicago, Illinois 60607, USA*
[46]*Northern Illinois University, DeKalb, Illinois 60115, USA*
[47]*Northwestern University, Evanston, Illinois 60208, USA*
[48]*Indiana University, Bloomington, Indiana 47405, USA*

[49]Purdue University Calumet, Hammond, Indiana 46323, USA
[50]University of Notre Dame, Notre Dame, Indiana 46556, USA
[51]Iowa State University, Ames, Iowa 50011, USA
[52]University of Kansas, Lawrence, Kansas 66045, USA
[53]Louisiana Tech University, Ruston, Louisiana 71272, USA
[54]Northeastern University, Boston, Massachusetts 02115, USA
[55]University of Michigan, Ann Arbor, Michigan 48109, USA
[56]Michigan State University, East Lansing, Michigan 48824, USA
[57]University of Mississippi, University, Mississippi 38677, USA
[58]University of Nebraska, Lincoln, Nebraska 68588, USA
[59]Rutgers University, Piscataway, New Jersey 08855, USA
[60]Princeton University, Princeton, New Jersey 08544, USA
[61]State University of New York, Buffalo, New York 14260, USA
[62]University of Rochester, Rochester, New York 14627, USA
[63]State University of New York, Stony Brook, New York 11794, USA
[64]Brookhaven National Laboratory, Upton, New York 11973, USA
[65]Langston University, Langston, Oklahoma 73050, USA
[66]University of Oklahoma, Norman, Oklahoma 73019, USA
[67]Oklahoma State University, Stillwater, Oklahoma 74078, USA
[68]Oregon State University, Corvallis, Oregon 97331, USA
[69]Brown University, Providence, Rhode Island 02912, USA
[70]University of Texas, Arlington, Texas 76019, USA
[71]Southern Methodist University, Dallas, Texas 75275, USA
[72]Rice University, Houston, Texas 77005, USA
[73]University of Virginia, Charlottesville, Virginia 22904, USA
[74]University of Washington, Seattle, Washington 98195, USA

[a]Deceased.
[b]Visitor from Augustana University, Sioux Falls, South Dakota 57197, USA.
[c]Visitor from The University of Liverpool, Liverpool L69 3BX, United Kingdom.
[d]Visitor from Deutshes Elektronen-Synchrotron (DESY), Notkestrasse 85, Germany.
[e]Visitor from CONACyT, M-03940 Mexico City, Mexico.
[f]Visitor from SLAC, Menlo Park, California 94025, USA.
[g]Visitor from University College London, London WC1E 6BT, United Kingdom.
[h]Visitor from Centro de Investigacion en Computacion—IPN, CP 07738 Mexico City, Mexico.
[i]Visitor from Universidade Estadual Paulista, São Paulo, São Paulo 01140, Brazil.
[j]Visitor from Karlsruher Institut für Technologie (KIT)—Steinbuch Centre for Computing (SCC), D-76128 Karlsruhe, Germany.
[k]Visitor from Office of Science, U.S. Department of Energy, Washington, DC 20585, USA.
[l]Visitor from University of Maryland, College Park, Maryland 20742, USA.
[m]Visitor from European Organization for Nuclear Research (CERN), CH-1211 Geneva, Switzerland.
[n]Visitor from Purdue University, West Lafayette, Indiana 47907, USA.
[o]Visitor from Institute of Physics, Belgrade, Belgrade, Serbia.
[p]Visitor from P. N. Lebedev Physical Institute of the Russian Academy of Sciences, 119991 Moscow, Russia.